ACS OMEGA

Open Access

http://pubs.acs.org/journal/acsodf

Article

Antibacterial Activity of Molybdenum Oxide−Polyacrylonitrile Composite Membrane with Fast Silver Ion Reduction

Muhammad Farooq, Muhammad Imran Bilal, Sabeen Gohar, Maira Khalid, Md. Kaiser Haider, and Ick Soo Kim*

Cite This: *ACS Omega* 2023, 8, 49467−49477

Read Online

ACCESS | Metrics & More | Article Recommendations | Supporting Information

ABSTRACT: The development of hybrid composite antibacterial agents for wound dressing has garnered significant attention due to their remarkable antibacterial efficacy and their potential to mitigate microbial resistance. In this study, we present an approach to designing and fabricating wound dressing membranes, utilizing molybdenum oxide−polyacrylonitrile (MoO_3/PAN) hybrid composites through electrospinning. Subsequently, we enhanced the membrane's effectiveness by introducing silver (Ag@MoO_3/PAN) into the matrix via a rapid (within one min) green synthesis method under UV irradiation. Initially, we discuss the morphological characteristics and structural attributes of the resulting membranes. Subsequent investigations explore the antibacterial mechanisms of both MoO_3 and Ag^+, revealing that the incorporation of silver substantially enhanced antibacterial activity. Additionally, we elucidate the surface properties, noting that the introduction of silver increases the surface area of the composite membrane by 25.89% compared with the pristine MoO_3/PAN membrane. Furthermore, we observe a 9% reduction in the water contact angle (WCA) for the Ag@MoO_3/PAN membrane, indicating improved hydrophilicity. Finally, we analyze the release behavior of the Ag@MoO_3/PAN membrane. Our findings demonstrate an initial burst release within the first 7 h, followed by a controlled and sustained release pattern over a period of 7 days.

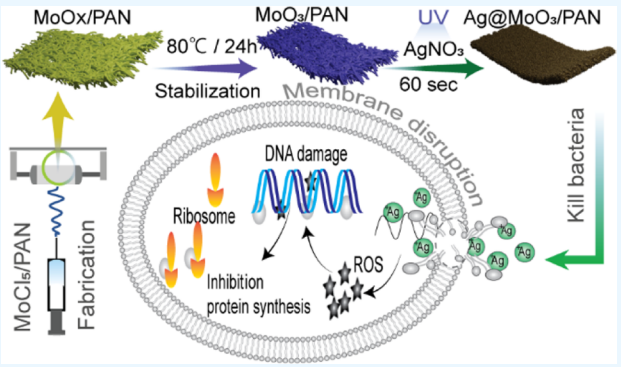

INTRODUCTION

The main purpose of a wound dressing is to create a healing environment for wounds while protecting them from damage and the invasion of harmful microorganisms. Whether it is a sutured wound resulting from surgery or trauma or an open wound preventing infections is a concern in wound care worldwide.[1,2] However, addressing infection control has become an issue due to the increasing number of microorganisms. Many bacteria have developed resistance to antibiotics, which focuses on the need to explore new materials for treating harmful microorganisms.[3−5] Through reduction in the production of new antibiotic materials or reduction of their usage, it is estimated that bacterial infections could cause around 10 million deaths by 2050.[6] Therefore, we must find new approaches to combat bacteria beyond relying on antibiotics. To tackle this challenge of preventing infections of microorganisms, there has been active research in alternative antibacterial technologies that could replace conventional remedial treatment.[7,8] Unlike antiseptic drugs that attack sites within the cells, metal-containing nanomaterials possess inherent passive antibacterial mechanisms that make them less prone to resistance. These mechanisms involve direct interactions with microorganisms, the release of metal ions that generate reactive oxygen species (ROS), and the indirect enhancement of ROS production that helps to combat bacteria.[7,9−11] Moreover, these nanomaterials possess properties that can be easily modified and tailored according to needs, making them more flexible compared to antibiotics. Despite the advantages of using metal-based nanomaterials for their passive antibacterial properties, they can still have some drawbacks. For instance, the uncontrolled and sustained release of metal ions can lead to the development of excessive ROS, which can cause various diseases. Moreover, the rapid deterioration of these materials can decrease their effectiveness over time.[12−14]

To address this challenge, hybrid nanomaterials are being employed, which combine various nanomaterials to enhance antibacterial efficacy and mitigate the risk of resistance development.[15] By the creation of hybrid composites, it becomes possible to maximize the advantages while minimizing the drawbacks associated with individual types of

Received: November 6, 2023
Revised: November 21, 2023
Accepted: November 24, 2023
Published: December 11, 2023

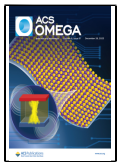

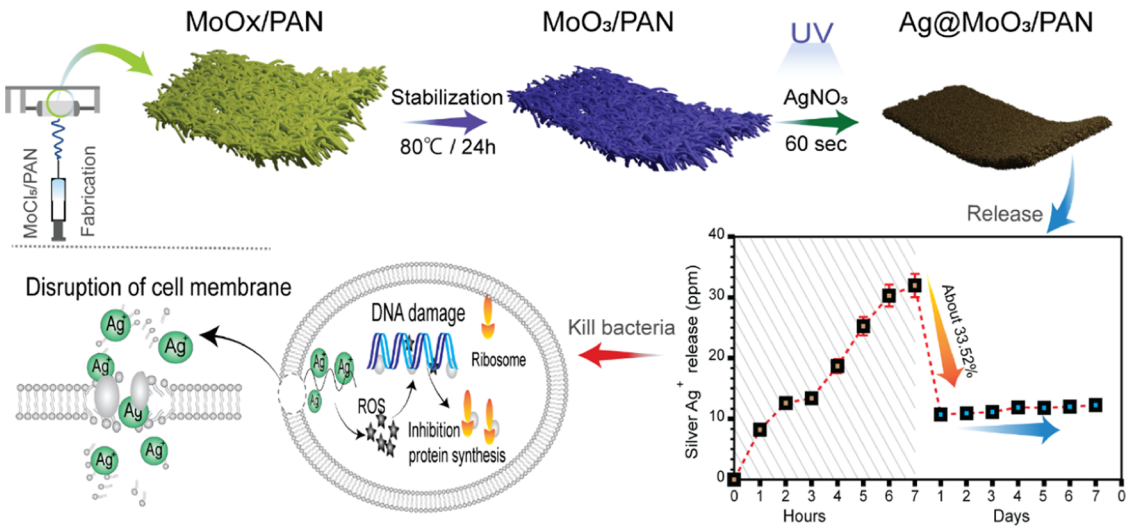

Figure 1. Graphical representation of silver nanoparticles doped on the surface of the MoO_3/PAN composite membrane with silver release profile and schematic illustration of bacterial death with silver ions.

nanoparticles (NPs). Additionally, the "combinatorial" approach allows for an extended duration of effective antibacterial action, significantly reducing bacterial resistance development.[10,16] Among the diverse array of nanomaterials available, organic polymerized nanomaterials offer the advantage of pH-responsive antimicrobial properties and the ability to mimic the actions of antimicrobial peptides to combat bacteria.[17,18] Inorganic metals,[7,19] such as gold[20,21] (Au), silver[22,23] (Ag), and copper[24,25] (Cu), as well as transition metal dichalcogenides[26] (TMDs), metal oxides,[27,28] carbon-based nanomaterials,[29] polymers, and their nanocomposites, have all been prominently utilized in the antibacterial research field.[30] These materials operate through distinct antibacterial mechanisms compared with conventional antibiotics and carry a reduced risk of fostering bacterial resistance. Consequently, the utilization of nanomaterials holds significant promise as an alternative to antibiotics for combating drug-resistant bacteria.

In various inorganic materials, molybdenum (Mo)-based nanomaterials have gained significant attention in the antibacterial research field due to their distinctive physicochemical properties.[31−33] Mo also serves as an essential trace element for microorganisms, plants, and animals.[9] Furthermore, within organisms, Mo functions as a cofactor for numerous enzymes (such as aldehyde, xanthine, and sulfite oxidase), participating in metabolic processes and facilitating various physiological functions, including protein synthesis.[34,35] One highly promising antibacterial nanomaterial is molybdenum trioxide (MoO_3).[36] Its antimicrobial mechanism in the presence of water involves a dissolving process, resulting in an acidic reaction and the formation of hydronium (H_3O^+) and molybdate (MoO_4^{2-}) ions. The infiltration of a hydronium (H_3O^+) ion through the bacterial cell wall disrupts the pH balance, enzyme activity, and transport systems within the cell. This acidic, low-pH environment induced by MoO_3 nanoparticles has been reported as an effective antimicrobial agent against susceptible and resistant strains of bacteria.[37] The penetration of hydroxonium ions through cell membranes hindered cell proliferation, affecting enzymes and transport systems, thereby slowing down the growth of bacteria and fungi.[38]

In addition to its antibacterial properties, MoO_{3-x} can also be combined with other materials to synthesize functionalized nanocomposites, which can generate synergistic antibacterial effects.[39] Silver ions Ag^+ have long been recognized as effective antimicrobial agents with low toxicity to humans and extensively studied in various in vitro and in vivo applications.[40] Silver molybdates have been explored in fields, such as lubrication,[41] humidity, gas sensors, photoelectronic devices,[41,42] and surface-enhanced Raman scattering techniques.[43] While the release of Ag^+ in wound dressings is a common practice with several benefits in wound care, it is crucial to control the release to prevent potential harm from excessive Ag^+ release.[12,44]

In addressing the issue of excessive silver ion release and its potential environmental impact, the molybdenum−PAN (MoO_3/PAN) membrane can serve as a key element to absorb and sequester these silver ions, preventing their release into the environment.[45] Additionally, it can create a moderately moist wound healing environment while effectively controlling the release of silver ions to achieve antibacterial effects.[46] Previous research conducted by our team has confirmed the efficacy of molybdenum trioxide nanoparticles (NPs) embedded in polyacrylonitrile (PAN) in promoting wound healing and controlling the release of silver ions for antibacterial purposes.[47] Notably, these NPs have exhibited highly promising antimicrobial properties against both *Bacillus subtilis* and *Escherichia coli*.

In this current study, we introduce a novel hybrid composite named the MoO_3/PAN membrane, which doped silver nanoparticles through a green fast synthesis approach mediated by UV light. To assess the antibacterial efficacy of this nanocomposite, we employed representative bacterial models, including *E. coli* and *B. subtilis*. That revealed a correlation between the silver content of the nanocomposites and their antibacterial effectiveness. Furthermore, we assessed controlled silver ion release, a crucial aspect of this research. These findings illustrate an outstanding advancement in the field of antibacterial materials and hold the potential to revolutionize wound dressings. A graphical representation of this study is shown in Figure 1.

https://doi.org/10.1021/acsomega.3c08814
ACS Omega 2023, 8, 49467−49477

RESULTS AND DISCUSSION

The synthesis of the MoO_3/PAN composite membrane followed previous reports[48] on the WO_3/PAN membrane with slight modifications, as detailed in the Experimental Section of the Supporting Information. The incorporation of silver into the MoO_3/PAN composite membrane was synthesized through a rapid green synthesis method within one min under UV light. The crystalline structures of both the MoO_3/PAN composite membrane, as shown in Figure 2a, and the Ag@MoO_3/PAN membrane, displayed in Figure 2b, were analyzed by using X-ray diffraction (XRD). In the MoO_3–PAN composite membrane, prominent peaks were observed at 9.6, 16.69, 19.30, 25.65, 29.25, and 35.31°, corresponding to the (100), (110), (200), (210), (111), and (211) planes, respectively. These findings align with the JCPDS reference number (JCPDS No. 00-065-0033) and confirm the molybdenum oxide membrane. After the introduction of silver nitrate ($AgNO_3$) into the MoO_3/PAN composite membrane under UV light, XRD analysis confirmed the conversion of the ions into metallic silver. Strong corresponding peaks were observed at 27.21, 32.03, 33.49, 38.87, 48.09, 51.22, and 56.14°, corresponding to the (220), (311), (222), (400), (422), (511), and (440) planes of silver molybdenum oxide (Ag_2MoO_4). These peaks matched the JCPDS reference number (JCPDS No. 01-075-0250). Importantly, no additional peaks were observed, confirming the absence of other impurities and attesting to the excellent crystalline quality of the Ag@MoO_3–PAN composite membrane. A typical polyacrylonitrile PAN peak was observed near 17.50°.[49]

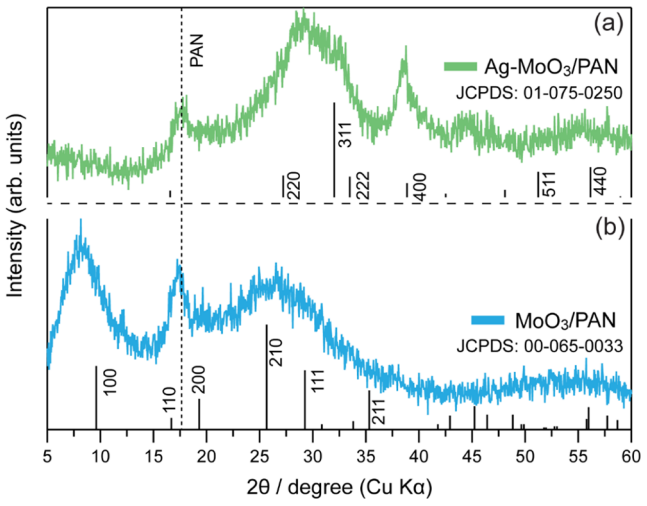

Figure 2. XRD diffraction patterns with (a) representing the MoO_3/PAN composite membrane and (b) corresponding to the Ag@MoO_3/PAN membrane after silver doping.

The morphology of the MoO_3/PAN nanofiber composite was characterized using scanning electron microscopy (SEM), as depicted in Figure 3a, while Figure 3b illustrates the SEM analysis of the Ag@MoO_3/PAN membrane. SEM provides valuable insights into the membrane structure and their corresponding elemental distribution mappings. In the case of the MoO_3/PAN composite, the distribution of Mo and O elements appeared consistent and evenly dispersed, indicating a uniform mixture of the inorganic MoO_3 and organic components, resulting in a homogeneous phase. No other impurities were observed. Additionally, in the silver-deposited

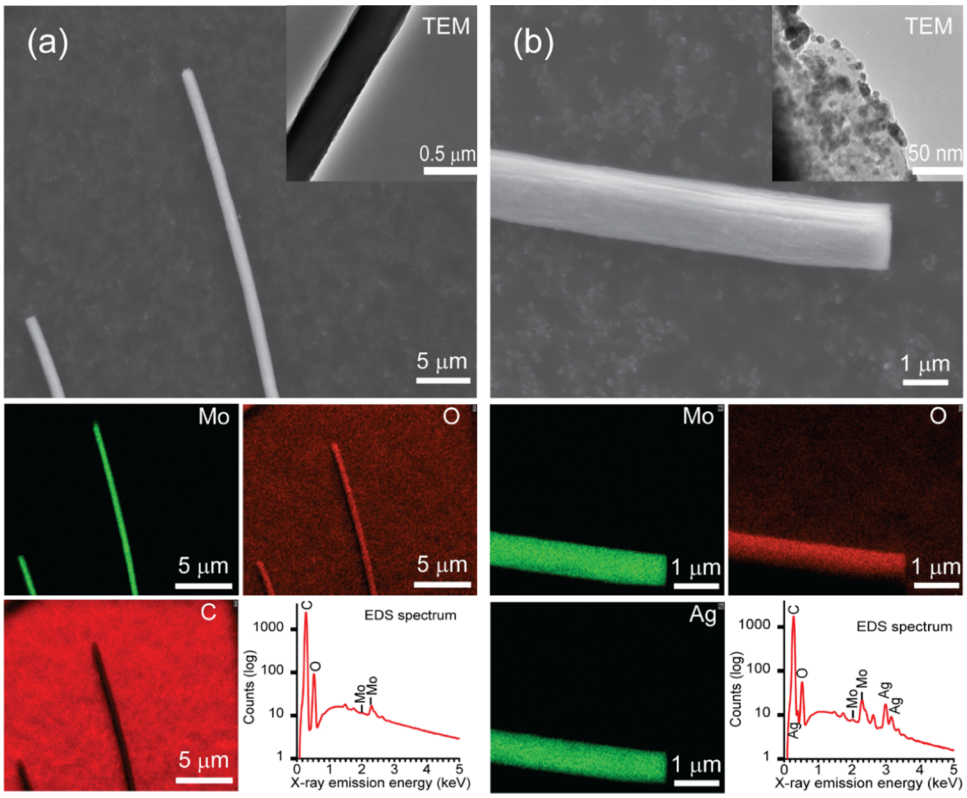

Figure 3. (a) SEM images of MoO_3/PAN and (b) SEM images of the Ag@MoO_3/PAN nanofiber membrane and their corresponding elemental mapping images of Mo, O, C, and Ag elements, and EDS spectrum and TEM images, respectively.

https://doi.org/10.1021/acsomega.3c08814
ACS Omega 2023, 8, 49467–49477

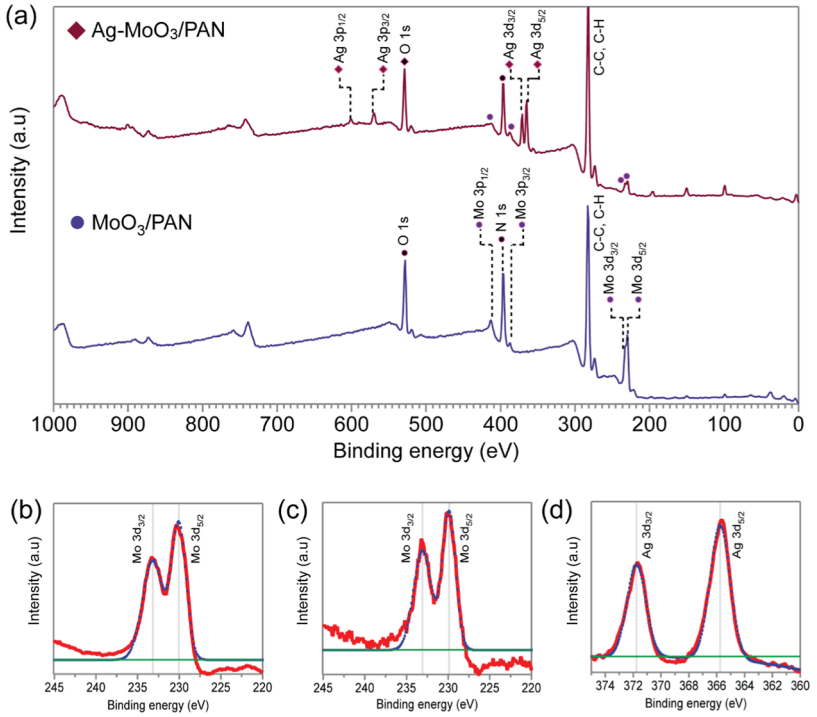

Figure 4. (a) Wide XPS spectrum of MoO_3/PAN and silver-doped membrane. High-resolution deconvoluted XPS spectrum for (b) Mo 3d for the MoO_3/PAN membrane, (c) Mo 3d for the Ag@MoO_3/PAN membrane, and (d) Ag 3d for the Ag@MoO_3/PAN membrane.

composite membrane, Ag was well-distributed across the membrane, as evidenced by the TEM image and elemental distribution, which revealed the presence of Mo, O, and Ag elements within the nanofibers. Furthermore, Figure 3 includes their energy-dispersive X-ray spectroscopy (EDS) spectra, while the comprehensive EDS spectra of MoO_3/PAN and Ag@MoO_3/PAN were presented (Figures S5 and S6, respectively).

XPS analysis was conducted to examine the surface elemental composition and chemical states of both the MoO_3/PAN membrane and the silver-doped composite membrane. The wideband spectra of both membranes, along with their corresponding Mo 3d and Ag 3d spectra, are depicted in Figure 4a,b. In the Mo 3d spectra of the membranes, it was observed that the Mo 3d doublet could be effectively fitted by using a Gaussian function. The primary contributing peaks at 230.0 and 233.1 eV corresponded to the characteristic values of the Mo^{5+} 3d doublet, and no minor peaks were detected. Figure 4c,d represents the Ag@MoO_3/PAN composite membrane and its corresponding Mo 3d and Ag 3d spectra, respectively. The introduction of silver nanoparticles did not result in any noticeable shifts in the Mo spectrum, indicating that the presence of silver did not affect the transition state of molybdenum.[47,50] In the Ag 3d spectra, the major contributor peaks at 365.8 and 371.9 eV exhibited slight shifts in binding energy toward lower values. This shift was attributed to the reduction of silver ions to metallic silver (Ag^0). The dominant peaks confirmed the presence of metallic silver, while no minor peaks were observed, implying the complete reduction of silver ions to the metallic state[22] (Ag^0). A prominent oxygen peak, around 532 eV, was evident in both membranes, substantiating the formation of MoO_3 and $AgMoO_4$. Additionally, the N 1s spectrum was observed in the range of 397−399 eV, corresponding to the binding energies of Mo 3p and Mo−N, as well as amine N bonds. These results indicated that molybdenum is not only physically adsorbed but also chemically bonded to polyacrylonitrile (PAN), forming Mo−N bonds. Consequently, a coexistence of amorphous and crystalline structures was established.[51]

FTIR spectra were conducted in the range of 400−4000 cm^{-1} to identify various functional groups, as illustrated in Figure 5. The presence of the nitrile group (C≡N) in PAN is

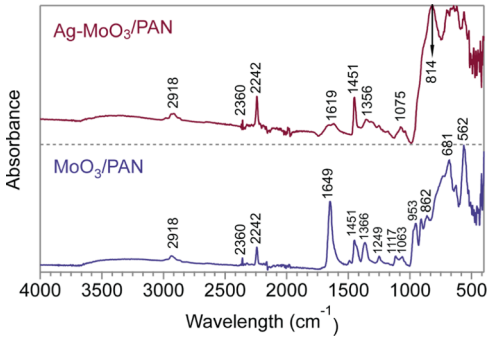

Figure 5. Fourier transform infrared analysis for the hybrid membrane of MoO_3/PAN and Ag@MoO_3/PAN.

indicated by the peak at 2242 cm^{-1}, while the bending and stretching vibrations of the $C-H_2$ functional group in PAN are represented by peaks at 1451 and 2918 cm^{-1}, respectively. Additionally, weak ether peaks (C−O−C) are observed at 1063 and 1249 cm^{-1}. Notably, the MoO_3 peak primarily appears below 1000 cm^{-1}. Peaks at 862 cm^{-1} correspond to the bending vibrational modes of Mo−O−Mo, while the peak at 562 cm^{-1} is attributed to the stretching mode vibration of the Mo−O−Mo entity.[51] Small peak shifts are observed, potentially arising from the composite nature of the MoO_3/PAN membrane. Upon the introduction of Ag into the MoO_3/

https://doi.org/10.1021/acsomega.3c08814
ACS Omega 2023, 8, 49467−49477

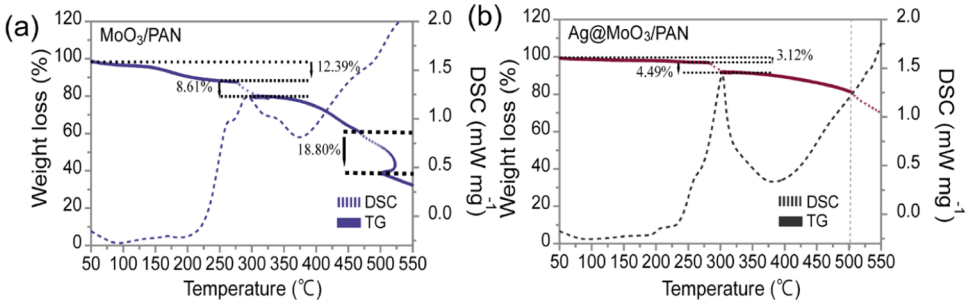

Figure 6. Thermogravimetric analysis of pure (a) MoO_3/PAN composite and (b) silver-doped composite membrane with their corresponding DSC curves.

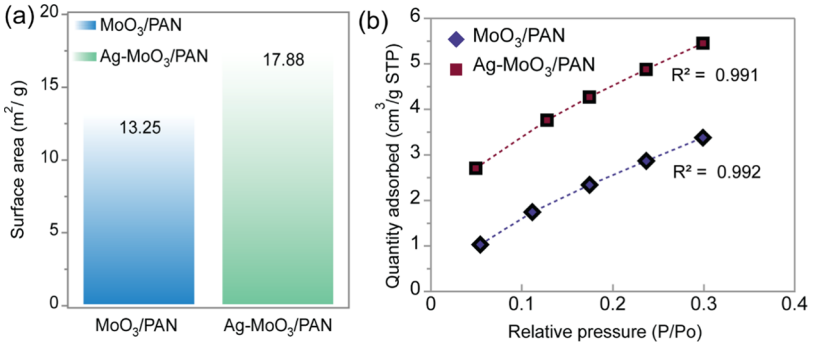

Figure 7. (a) BET surface area of both the MoO_3 and silver-doped membrane and (b) isotherm linear plot fit.

PAN membrane, significant changes occur, including the appearance of two new peaks at 1356 and 1619 cm^{-1}, accompanied by the disappearance of the Mo bending peak.[51] These changes suggest potential bonding interactions between molybdenum and silver.[52] Raman spectra are also shown (Figure S3).

Thermal gravimetric analysis (TGA) of the molybdenum nanocomposite is shown in Figure 6a, revealing distinct two-step weight loss events in the as-prepared membrane. The initial small weight loss was due to moisture evaporation. The initial weight loss occurring before 450 °C is attributed to the decomposition of the PAN component, while the subsequent stages, ranging from 450 to 550 °C, correspond to the dehydration and transformation of amorphous MoO_3 into a crystalline state.[38] Upon the introduction of silver nanoparticles into the composite, as shown in Figure 6b, the T_g shifts toward 500 °C. This shift in T_g toward a higher temperature range is attributed to increased lateral forces within the bulk state, which might be due to the restricted steric effect[53] (TGA analysis of 10% PAN is shown in Figure S4).

The BET analysis of the as-prepared membrane is conducted using N_2 adsorption and desorption kinetics.[54] Figure 7a presents the BET surface area data. The surface area for MoO_3 measures approximately 13.25 m^2/g. Notably, upon incorporation of silver nanoparticles into the membrane, the surface area increased by 23.89% as compared to the pristine MoO_3/PAN membrane. This enhancement of the area can be attributed to the enlargement of nanofiber diameter, as verified by SEM images larger nanofibers provide a greater surface area. There could be a chemical interaction of silver nanoparticles on the surface of the membrane, such as the adsorption of gas molecules onto the silver nanoparticles themselves.[55] The linear plot fit coefficient factor R^2 for the isotherm analysis was determined to be 0.991, indicating a good fit with the values displayed in Figure 7b.

The DPPH antioxidant assay for the prepared nanofiber membrane was conducted using the 2,2-diphenyl-1-picrylhydrazyl (DPPH) free radical scavenging method. To assess the antioxidant activity of the produced fibers, a 30 mg sample of the fiber was combined with 100 μL of DPPH solution in ethanol and 80 μL of assay buffer. This mixture was then incubated for various time intervals: specifically, 0.5 1, 2, 3, 4, 5, 6, and 7 h. After each specified incubation period, the absorbance at 517 nm was measured by using a UV−vis spectrophotometer (Lambda 900, PerkinElmer). The DPPH free radical scavenging activity was calculated as a percentage using eq 1[56]

$$\text{scavenging activity } (\%) = \frac{A_c - A_s}{A_c} \times 100 \quad (1)$$

where Ac (control) and A_s (sample) is the absorbance of DPPH solutions without and with nanofiber mats at 517 nm.

Figure 8 presents the assessment of the antioxidant activity of the prepared MoO_3/PAN nanofiber membranes utilizing ethanol as the solvent for the DPPH scavenging assay. MoO_3, as a composite material, is recognized for its antioxidant properties,[34,57] yielding an initial activity of approximately 62% after a 30 min evaluation. Interestingly, after 7 h, this percentage only increased by 2% compared to the initial 30 min measurement. Conversely, the silver-doped MoO_3 composite membrane initially exhibited relatively low antioxidant activity, measuring approximately 15%. This reduction in activity could potentially be attributed to the presence of silver metal incorporated into the MoO_3 composite material.[58] Indeed, it seemed that the presence of silver applied an inhibitory effect on the antioxidant activity of MoO_3/PAN, possibly involving chemical interactions with the MoO_3/PAN

https://doi.org/10.1021/acsomega.3c08814
ACS Omega 2023, 8, 49467−49477

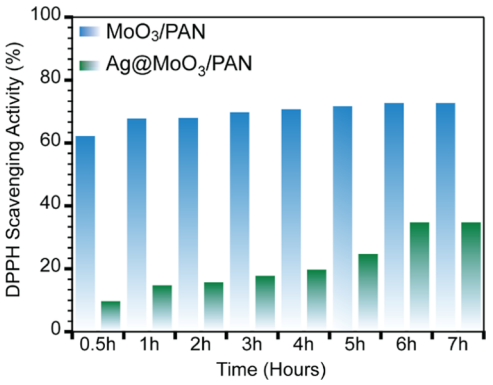

Figure 8. DPPH free radical scavenging activity of the MoO_3/PAN composite membrane and silver-doped composite membrane.

components. Over time, the scavenging activity increased by approximately 30%, which may be associated with the gradual release of silver ions and potential oxidation of the DPPH molecules themselves.[59,60]

Antimicrobial assessments were conducted using a method explained in our previous research.[47] To evaluate the antimicrobial properties of the produced fibers, we employed the agar disc diffusion assay following the standard test method (AATCC 147-1998). Specifically, bacterial strains, *E. coli* and *B. subtilis*, were utilized for the experiment. In this assay, we applied 25 μL of a 10^{-5} dilution of the bacterial strains onto sterile agar plates. Subsequently, two fiber samples were cut into 10 mm round shapes and gently positioned on the agar surface. Gentle pressure was applied to ensure close contact between the fibers and the agar. The plates were then incubated at 37 °C for 20 h. Figure 9a–c visually demonstrates the antibacterial activity of the MoO_3/PAN nanofiber membranes, as evidenced by the presence of inhibition zones on the corresponding agar plates. These inhibition zones serve as indicators of the membrane's efficacy in impeding the growth of both *E. coli* and *B. subtilis* bacteria. The mechanism underlying bacterial death is attributed to hydroxonium ions.[36] Initially, molybdenum trioxide (MoO_3) reacts with water to form molybdic acid (H_2MoO_4). Upon contact with water, molybdic acid releases hydroxonium ions (H_3O^+). These hydroxonium ions interact with the bacterial cell membrane, causing DNA damage, inhibiting the synthesis of new proteins, and ultimately resulting in cell destruction, as schematically demonstrated in Figure 9d. At equilibrium, hydroxonium ions are transformed back into molybdic acid.[61]

The introduction of silver, referred to as "silver doping," further enhances the inhibition of bacterial viability, especially in the case of *E. coli*. Ag^+ ions are released from the Ag@MoO_3/PAN membrane and interact with the cell membranes of both *E. coli* and *B. subtilis*, leading to the disruption of these bacterial cell membranes. AgNPs exhibit antibacterial effects by binding to bacterial surfaces and subsequently penetrating the

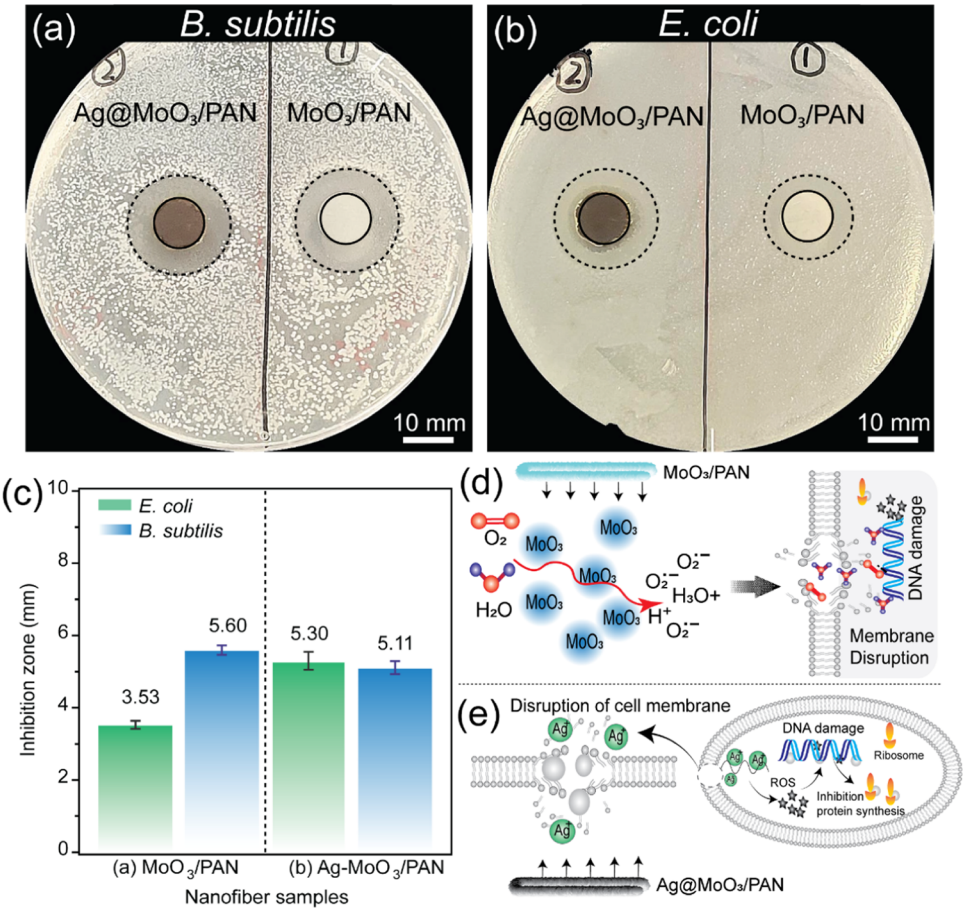

Figure 9. (a) *B. subtilis* agar plates of antibacterial performance by inhibition zone diameter. (b) *E. coli* agar plate, (c) inhibition zone diameter of as-prepared nanofiber membranes, (d) schematic illustration of bacteria-killing behaviors of Ag@MoO_3/PAN, and (e) schematic illustration of bacteria-killing behaviors by the MoO_3/PAN composite nanofiber membrane.

https://doi.org/10.1021/acsomega.3c08814
ACS Omega 2023, 8, 49467−49477

bacteria to modulate their activities by dephosphorylating tyrosine residues.[13,62] It is widely accepted that protein dephosphorylation can inhibit the enzyme activity. When the activity of enzymes related to bacterial growth is inhibited, the behavior of the bacteria is disrupted or altered.[63] Concurrently, this interaction damages DNA and ribosomes, resulting in cell death, as illustrated in Figure 9e. This effect is particularly pronounced in the case of *E. coli*, where the inhibition zone is larger for the Ag@MoO_3/PAN composite nanofiber membrane compared to the MoO_3/PAN composite nanofiber membrane.

Water contact angle (WCA) is shown in Table 1, with the MoO_3/PAN composite nanofiber membrane exhibiting contact angles of approximately 77°. These angles indicate the hydrophilic nature of the material, facilitating enhanced absorption of wound exudate.[64] This property helps maintain a moist wound environment, preventing the formation of a dry scab. Upon introduction of silver into the MoO_3/PAN composite, the water contact angle decreases by 9%. This reduction can likely be attributed to the higher surface area of the membrane, as confirmed by our BET surface area measurements. Consequently, the Ag@MoO_3/PAN nanofiber membrane exhibits improved wettability, enhancing its ability to interact with liquids.

Table 1. Water Contact Angle of the As-Prepared MoO_3/PAN Composite Membrane and Silver-Dopped Ag@MoO_3/PAN Membrane

nanofiber membranes	water contact angle (θ)
MoO_3/PAN	77°
Ag-MoO_3/PAN	70°

The release profile of Ag^+ ions plays a crucial role in determining the antibacterial activity of Ag-incorporated nanofiber membranes (NFMs).[12] We conducted an evaluation to quantify the release rates and amounts of silver (ppm) from Ag-MoO_3/PAN membranes, as illustrated in Figure 10a. To assess the release behavior across Ag-MoO_3/PAN samples, we employed inductively coupled plasma optical emission spectroscopy (ICP-OES) and prepared standard solutions with silver concentrations of 0.5, 1, 5, 10, and 20 ppm to establish a calibration curve. The coefficient factor R^2 was determined to be 0.999, as shown in Figure 10b. This procedure for measuring the release profile aligns with previous reports.

When it comes to traditional silver nanoparticles (AgNPs) and nanomaterials loaded with AgNPs, it is not easy to control how silver ions are released. So, how effective these materials are at killing bacteria often depends on how much they are exposed to in each situation. Initially, having a lot of silver ions inside bacteria helps to quickly and effectively eliminate the bacteria and hinders microorganisms from being resistant against antibiotic materials.[12,44] After the initial burst, there must be control and maintenance of silver release, and excessive silver will not damage the skin.[65] The release of these silver ions from materials containing AgNPs usually happens slowly or rapidly increases continuously.[66] This is why it is important to find ways to initially increase the amount of silver ions and then steadily maintain the release of ions.

The results indicate that the release of silver ions is controlled by the MoO_3/PAN composite membrane. These results show that initially, there is a rapid release of silver ions within the first 7 h, followed by a significant decrease in the release rate after 1 day. During the initial 7 h, there is a continuous increase in silver ion release, reaching a peak of 31.95 ppm. However, after the initial burst, there is a

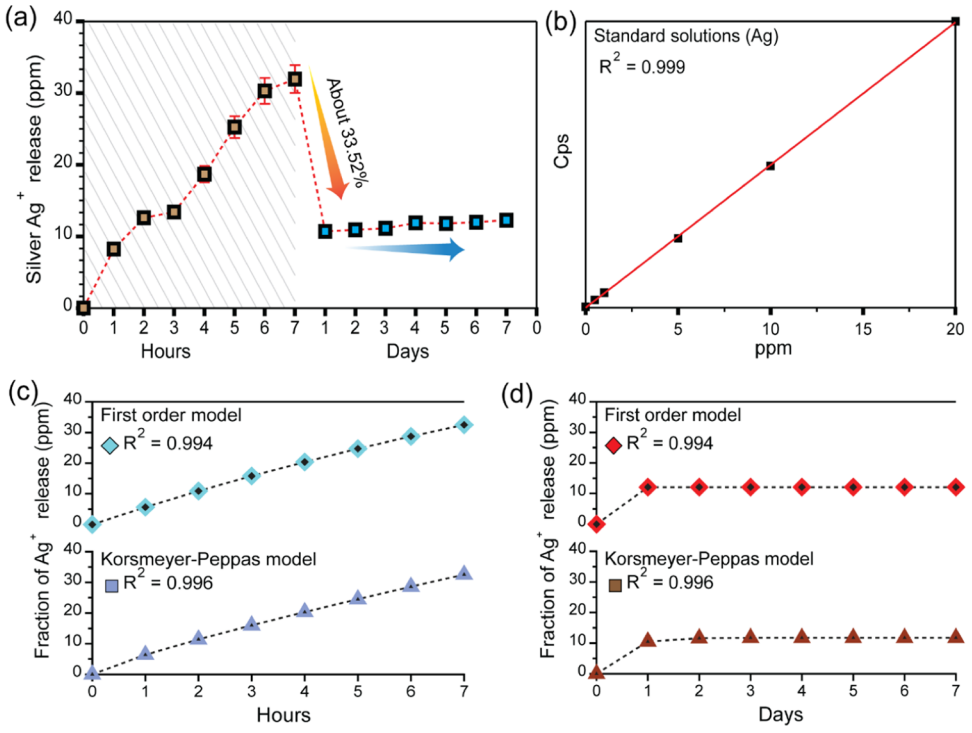

Figure 10. (a) Silver release of the Ag@MoO_3/PAN nanofiber membrane, (b) standard solution of Ag with different concentrations, and (c, d) first-order and Peppas model fitted curves of silver release data of hours and days, respectively. The error bars correspond to the standard deviation of three measurements.

https://doi.org/10.1021/acsomega.3c08814
ACS Omega 2023, 8, 49467−49477

noticeable decrease in the rate of silver ion release. At the end of the 1st day, the release was 10.71 ppm, which is a 33.56% reduction from the peak value. The release then remains relatively stable with minor fluctuations over the next 7 days. This reduction in silver ion release rate after the initial burst could be attributed to the MoO_3/PAN composite membrane having functional groups that can interact with silver ions. These interactions can lead to the binding or complexation of silver ions on the membrane surface or within its structure.[9,63] This binding reduces the concentration of free silver ions available for release. Additionally, at the start, the membrane has many available binding sites for silver ions, but over time, these binding sites might be decreased, resulting in reduced release.[45,47,67]

Furthermore, we analyzed the release data of the Ag@MoO_3/PAN composite membrane using different models, as described in a previous report.[68] The release data showed a better fit with the Peppas and first-order models, as shown in Figure 10c for hours and Figure 10d for days release, suggesting that multiple mechanisms may be involved in the release process. The Korsmeyer−Peppas model is a general approach used to describe the release of drugs and other substances.[69]

$$F = kt^n \quad (2)$$

The drug, which is encapsulated within porous materials, can be described by the first-order equation.[70]

$$F = 1 - e^{-kt} \quad (3)$$

CONCLUSIONS

In summary, we have successfully synthesized a hybrid composite material comprising molybdenum oxide and polyacrylonitrile (MoO_3/PAN) through electrospinning. Additionally, we have developed a rapid green synthesis method that can reduce silver ions to metallic silver on the surface of the composite material within one min, resulting in the formation of a Ag@MoO_3/PAN membrane. Our research has confirmed that molybdenum oxide exhibits highly effective antimicrobial activity against both *E. coli* and *B. subtilis* bacteria. Furthermore, the incorporation of silver nanoparticles into the composite material has enhanced its antibacterial properties, particularly against *E. coli* bacteria. Moreover, we have increased the surface area of the molybdenum composite material by 25.89% through the incorporation of silver nanoparticles, leading to a 9% improvement in surface wettability. We have also addressed the issue of uncontrolled silver release by this new composite hybrid material of MoO_3/PAN, reducing the excessive release of silver ions by 33.52% within 24 h. This intelligent hybrid material, Ag@MoO_3/PAN, has also proven to be effective in combating multidrug-resistant bacterial strains. We firmly believe that this study opens possibilities for extensive research, not only in the field of antimicrobial activity but also in other applications such as water filtration and the use of MoO_3/PAN membranes as surface-enhanced Raman spectroscopy (SERS) substrates. These applications can be further optimized by controlling the morphology of the materials.

EXPERIMENTAL SECTION

Materials. All chemicals were of analytical grade and used as received without further purification. Molybdenum pentachloride ($MoCl_5$) and PAN (MW 150,000 g/mol) were purchased from Sigma-Aldrich, Tokyo, Japan. *N*,*N*-dimethylformamide (DMF, 99.8%) and silver nitrate ($AgNO_3$, 99.8%) were purchased from FUJIFILM Wako Pure Chemical Ltd., Japan. *E. coli* (Hrf 3000) was provided from the Coli Genetic Stock (CGSC; Yale University, New Haven, CT). *B. subtilis* (168) was provided from Dr. Ogasawara, Shinshu University, Japan. Luria−Bertani broth was supplied in an analytical grade from Nacalai Tesque, Inc., Kyoto, Japan. The Petri dishes were purchased from Sansei Medical Co., Ltd., Japan. Milli-Q water (Direct-Q UV3) was used in the experiments.

Characterization. Field-emission scanning electron microscopy (FE-SEM; JSM-IT800SHL) and high-resolution transmission electron microscopy (TEM; JEOL, JEOL2010; accelerating voltage, 200 kV) were used to record the morphology and elemental composition of the membrane. Crystal structuring was characterized by X-ray diffraction (XRD; Rigaku, MiniFlex300) with monochromatic Cu Kα radiation at 33 kV. Fourier transform infrared (FT/IR-6600) and X-ray photoelectron spectroscopy (XPS, AXIS-ULTRA HSA SV) analyses were performed to thoroughly characterize the chemical structure and morphology of NFMs. For FTIR analysis, 72 scans at a resolution of 4 cm^{-1} were performed for each sample, and all spectra were presented in the wavenumber range 400−4000 cm^{-1}. Thermogravimetric analysis (Thermo plus TG-8120) of polymers was measured as a weight change analysis. Silver release content was measured by inductively coupled plasma optical emission spectrometry (ICP-OES, SPS 5000). An ultraviolet (UV) lamp light (WFH-204B, Shanghai Int.) was used as a reducing agent.

Membrane Fabrication. For the synthesis of the MoO_3−polyacrylonitrile (PAN) composite membrane, a typical procedure was employed. Initially, a solution was prepared by dissolving 10% PAN in 10 cm^3 dimethylformamide (DMF), resulting in a transparent solution. Subsequently, 60% of molybdenum pentachloride ($MoCl_5$) relative to the polymer content was introduced into the 10% polymer solution with vigorous stirring. The reaction occurred under ambient conditions, where the presence of atmospheric oxygen and residual water in DMF facilitated the oxidation and hydration of $MoCl_5$ precursors. During the initial 3 min of the reaction, the generation of white smoke, primarily composed of hydrogen chloride (HCl) gas, was observed continuously. Within 5 min, the solution underwent a transition from being colorless to exhibiting a jacinth hue and eventually transformed into a blue coloration. This change in color was attributed to the formation of numerous small clusters of MoO_3. Once the dispersion process was complete, the solution was loaded into a 10 mL plastic syringe equipped with a needle with a diameter of 0.7 mm. A syringe pump was operated at a flow rate of 0.8 mL h^{-1}, with the collector positioned at 18.0 cm from the needle. An applied voltage of 20 kV was maintained throughout the process. The humidity was controlled at 40 ± 5%. The electrospun fibrous membranes initially appeared to be yellow in color. Subsequently, these membranes were carefully detached from the substrate and subjected to vacuum drying at 80 °C for a duration of 24 h. This drying process served the dual purpose of removing DMF and enabling the formation of a stable MoO_3/PAN membrane. Notably, this membrane underwent a color transition from yellow to blue during the drying process. The resultant blue nanofiber membranes were then ready for subsequent characterization and analysis. The photoreduced, blue-colored membrane was submerged in a 0.1 M silver nitrate ($AgNO_3$) solution under

https://doi.org/10.1021/acsomega.3c08814
ACS Omega 2023, 8, 49467−49477

UV light, leading to the spontaneous reduction and deposition of silver nanoparticles (AgNPs) onto the membrane.

■ ASSOCIATED CONTENT

Supporting Information

The Supporting Information is available free of charge at https://pubs.acs.org/doi/10.1021/acsomega.3c08814.

Raman spectroscopy analysis, and other additional figures (PDF)

■ AUTHOR INFORMATION

Corresponding Author

Ick Soo Kim − *Graduate School of Medicine, Science and Technology, Shinshu University, Ueda, Nagano 386-8567, Japan; Nano Fusion Technology Research Group, Institute for Fiber Engineering (IFES), Interdisciplinary Cluster for Cutting Edge Research (ICCER), Shinshu University, Ueda, Nagano 386-8567, Japan;* orcid.org/0000-0003-2126-0381; Email: kim@shinshu-u.ac.jp

Authors

Muhammad Farooq − *Graduate School of Medicine, Science and Technology, Shinshu University, Ueda, Nagano 386-8567, Japan; Nano Fusion Technology Research Group, Institute for Fiber Engineering (IFES), Interdisciplinary Cluster for Cutting Edge Research (ICCER), Shinshu University, Ueda, Nagano 386-8567, Japan*

Muhammad Imran Bilal − *Department of Chemistry, School of Science, University of Management and Technology, Lahore 54770, Pakistan*

Sabeen Gohar − *Graduate School of Medicine, Science and Technology, Shinshu University, Ueda, Nagano 386-8567, Japan; Nano Fusion Technology Research Group, Institute for Fiber Engineering (IFES), Interdisciplinary Cluster for Cutting Edge Research (ICCER), Shinshu University, Ueda, Nagano 386-8567, Japan*

Maira Khalid − *Graduate School of Medicine, Science and Technology, Shinshu University, Ueda, Nagano 386-8567, Japan; Nano Fusion Technology Research Group, Institute for Fiber Engineering (IFES), Interdisciplinary Cluster for Cutting Edge Research (ICCER), Shinshu University, Ueda, Nagano 386-8567, Japan*

Md. Kaiser Haider − *Graduate School of Medicine, Science and Technology, Shinshu University, Ueda, Nagano 386-8567, Japan; Nano Fusion Technology Research Group, Institute for Fiber Engineering (IFES), Interdisciplinary Cluster for Cutting Edge Research (ICCER), Shinshu University, Ueda, Nagano 386-8567, Japan*

Complete contact information is available at: https://pubs.acs.org/10.1021/acsomega.3c08814

Author Contributions

M.F.: Conceptualization (lead), methodology, experimental and characterization (lead), writing—original draft (lead), investigation (lead), visualization (lead), data curation (lead), writing—review and editing (lead). M.I.B.: Visualization (supporting), formal analysis (supporting), and data curation (equal). S.G.: Visualization (supporting), dormal analysis (supporting), and data curation (supporting). M.K.: Visualization (supporting) and formal analysis (supporting). M.K.H.: Formal analysis (supporting). I.S.K.: Validation, resource, and supervisor.

Notes

The authors declare no competing financial interest.

■ ACKNOWLEDGMENTS

No funding was provided for this project. M.F. acknowledges JST SPRING Next-generation Advanced Human Resources/ Local Leader Development Program, Grant Number JPMJSP2144 (Shinshu University). M.F. is grateful to Prof. Murakami Yasushi (Shinshu University) for productive and valuable discussions regarding the synthesis. M.F. thanks Muhammad Nauman Sarwar and Yabuta Yoshinori (Shinshu University) for their support with the characterization and antibacterial activity.

■ REFERENCES

(1) Santos, F. G.; Bonkovoski, L. C.; Garcia, F. P.; Cellet, T. S. P.; Witt, M. A.; Nakamura, C. V.; Rubira, A. F.; Muniz, E. C. Antibacterial Performance of a PCL-PDMAEMA Blend Nanofiber-Based Scaffold Enhanced with Immobilized Silver Nanoparticles. *ACS Appl. Mater. Interfaces* **2017**, *9* (11), 9304−9314.

(2) Dreifke, M. B.; Jayasuriya, A. A.; Jayasuriya, A. C. Current Wound Healing Procedures and Potential Care. *Mater. Sci. Eng. C* **2015**, *48*, 651−662.

(3) Mulani, M. S.; Kamble, E. E.; Kumkar, S. N.; Tawre, M. S.; Pardesi, K. R. Emerging Strategies to Combat ESKAPE Pathogens in the Era of Antimicrobial Resistance: A Review. *Front. Microbiol.* **2019**, *10*, 539.

(4) De Oliveira, D. M. P.; Forde, B. M.; Kidd, T. J.; Harris, P. N. A.; Schembri, M. A.; Beatson, S. A.; Paterson, D. L.; Walker, M. J. Antimicrobial Resistance in ESKAPE Pathogens. *Clin. Microbiol. Rev.* **2020**, *33* (3), No. e00181-19.

(5) Mancuso, G.; Midiri, A.; Gerace, E.; Biondo, C. Bacterial Antibiotic Resistance: The Most Critical Pathogens. *Pathogens* **2021**, *10* (10), No. 1310, DOI: 10.3390/pathogens10101310.

(6) de Kraker, M. E. A.; Stewardson, A. J.; Harbarth, S. Will 10 Million People Die a Year Due to Antimicrobial Resistance by 2050? *PLoS Med.* **2016**, *13* (11), No. e1002184, DOI: 10.1371/journal.pmed.1002184.

(7) Frei, A.; Verderosa, A. D.; Elliott, A. G.; Zuegg, J.; Blaskovich, M. A. T. Metals to Combat Antimicrobial Resistance. *Nat. Rev. Chem.* **2023**, *7* (3), 202−224.

(8) Jia, B.; Li, G.; Cao, E.; Luo, J.; Zhao, X.; Huang, H. Recent Progress of Antibacterial Hydrogels in Wound Dressings. *Mater. Today Bio* **2023**, *19*, No. 100582.

(9) Liao, J.; Wang, L.; Ding, S.; Tian, G.; Hu, H.; Wang, Q.; Yin, W. Molybdenum-Based Antimicrobial Nanomaterials: A Comprehensive Review. *Nano Today* **2023**, *50*, No. 101875.

(10) Zhou, Z.; Li, B.; Liu, X.; Li, Z.; Zhu, S.; Liang, Y.; Cui, Z.; Wu, S. Recent Progress in Photocatalytic Antibacterial. *ACS Appl. Bio Mater.* **2021**, *4* (5), 3909−3936.

(11) Serag, E.; El-Aziz, A. M. A.; El-Maghraby, A.; Taha, N. A. Electrospun Non-Wovens Potential Wound Dressing Material Based on Polyacrylonitrile/Chicken Feathers Keratin Nanofiber. *Sci. Rep.* **2022**, *12* (1), No. 15460.

(12) Xu, Z.; Zhang, C.; Wang, X.; Liu, D. Release Strategies of Silver Ions from Materials for Bacterial Killing. *ACS Appl. Bio Mater.* **2021**, *4* (5), 3985−3999.

(13) Xu, F.; Piett, C.; Farkas, S.; Qazzaz, M.; Syed, N. I. Silver Nanoparticles (AgNPs) Cause Degeneration of Cytoskeleton and Disrupt Synaptic Machinery of Cultured Cortical Neurons. *Mol. Brain* **2013**, *6* (1), 29.

(14) Wang, C.; Wang, W.; Zhang, L.; Zhong, S.; Yu, D. Electrospinning of PAN/Ag NPs Nanofiber Membrane with Antibacterial Properties. *J. Mater. Res.* **2019**, *34* (10), 1669−1677.

(15) Elhassan, E.; Devnarain, N.; Mohammed, M.; Govender, T.; Omolo, C. A. Engineering Hybrid Nanosystems for Efficient and

Targeted Delivery against Bacterial Infections. *J. Controlled Release* **2022**, *351*, 598−622.
(16) Jayakumar, A.; Mathew, S.; Radoor, S.; Kim, J. T.; Rhim, J. W.; Siengchin, S. Recent Advances in Two-Dimensional Nanomaterials: Properties, Antimicrobial, and Drug Delivery Application of Nanocomposites. *Mater. Today Chem.* **2023**, *30*, No. 101492.
(17) Guggenbichler, J. K.; Eberhardt, N.; Martinez, H. P.; Wildner, H. Substance with an Antimicrobial Effect. PCT Patent PCT/EP2007/009814, 2007.
(18) Stan, D.; Enciu, A.-M.; Mateescu, A. L.; Ion, A. C.; Brezeanu, A. C.; Stan, D.; Tanase, C. Natural Compounds With Antimicrobial and Antiviral Effect and Nanocarriers Used for Their Transportation. *Front. Pharmacol.* **2021**, *12*, No. 723233.
(19) Yousaf, A. B.; Imran, M.; Farooq, M.; Kausar, S.; Yasmeen, S.; Kasak, P. Graphitic Carbon Nitride Nanosheets Decorated with Zinc-Cadmium Sulfide for Type-II Heterojunctions for Photocatalytic Hydrogen Production. *Nanomaterials* **2023**, *13* (18), No. 2609, DOI: 10.3390/nano13182609.
(20) Rabiee, N.; Ahmadi, S.; Akhavan, O.; Luque, R. Silver and Gold Nanoparticles for Antimicrobial Purposes against Multi-Drug Resistance Bacteria. *Materials* **2022**, *15* (5), No. 1799, DOI: 10.3390/ma15051799.
(21) Rodríguez-León, E.; Rodríguez-Vázquez, B. E.; Martínez-Higuera, A.; Rodríguez-Beas, C.; Larios-Rodríguez, E.; Navarro, R. E.; López-Esparza, R.; Iñiguez-Palomares, R. A. Synthesis of Gold Nanoparticles Using Mimosa Tenuiflora Extract, Assessments of Cytotoxicity, Cellular Uptake, and Catalysis. *Nanoscale Res. Lett.* **2019**, *14* (1), 334.
(22) Zhang, S.; Tang, Y.; Vlahovic, B. A Review on Preparation and Applications of Silver-Containing Nanofibers. *Nanoscale Res. Lett.* **2016**, *11* (1), 80.
(23) Husanu, E.; Chiappe, C.; Bernardini, A.; Cappello, V.; Gemmi, M. Synthesis of Colloidal Ag Nanoparticles with Citrate Based Ionic Liquids as Reducing and Capping Agents. *Colloids Surf., A* **2018**, *538*, 506−512.
(24) Mishra, A.; Djoko, K. Y.; Lee, Y. H.; Lord, R. M.; Kaul, G.; Akhir, A.; Saxena, D.; Chopra, S.; Walton, J. W. Water-Soluble Copper Pyrithione Complexes with Cytotoxic and Antibacterial Activity. *Org. Biomol. Chem.* **2023**, *21* (12), 2539−2544.
(25) Khandelwal, M.; Kumawat, A.; Misra, K. P.; Khangarot, R. K. Efficient Antibacterial Activity in Copper Oxide Nanoparticles Biosynthesized via Jasminum Sambac Flower Extract. *Part. Sci. Technol.* **2023**, *41* (5), 640−652.
(26) Wang, Q.; Wang, H.; Zhang, T.; Hu, Z.; Xia, L.; Li, L.; Chen, J.; Jiang, S. Antibacterial Activity of Polyvinyl Alcohol/WO3Films Assisted by Near-Infrared Light and Its Application in Freshness Monitoring. *J. Agric. Food Chem.* **2021**, *69* (3), 1068−1078.
(27) Mustafa, Y. F. Modern Developments in the Application and Function of Metal/Metal Oxide Nanocomposite−Based Antibacterial Agents. *BioNanoScience* **2023**, *13* (2), 840−852.
(28) Imran, M.; Yousaf, A. B.; Farooq, M.; Kasak, P. Enhanced Z-Scheme Visible Light Photocatalytic Hydrogen Production over A-Bi2O3/CZS Heterostructure. *Int. J. Hydrogen Energy* **2018**, *43* (9), 4256−4264.
(29) Xin, Q.; Shah, H.; Nawaz, A.; Xie, W.; Akram, M. Z.; Batool, A.; Tian, L.; Jan, S. U.; Boddula, R.; Guo, B.; Liu, Q.; Gong, J. R. Antibacterial Carbon-Based Nanomaterials. *Adv. Mater.* **2019**, *31* (45), 1804838.
(30) Yuan, H.; Chen, L.; Hong, F. F. A Biodegradable Antibacterial Nanocomposite Based on Oxidized Bacterial Nanocellulose for Rapid Hemostasis and Wound Healing. *ACS Appl. Mater. Interfaces* **2020**, *12* (3), 3382−3392.
(31) Cao, W.; Yue, L.; Wang, Z. High Antibacterial Activity of Chitosan − Molybdenum Disulfide Nanocomposite. *Carbohydr. Polym.* **2019**, *215*, 226−234.
(32) Drobot, N. F.; Noskova, O. A.; Ovchinnikova, N. A.; Zvereva, G. A.; Larin, G. M.; Krenev, V. A.; Trifonova, E. N.; Drobot, D. V. Complex Formation during Molybdenum Chlorination in DMF Medium. *Russ. J. Coord. Chem.* **2003**, *29* (7), 474−477.
(33) Yousaf, A. B.; Imran, M.; Farooq, M.; Kasak, P. Synergistic Effect of Co-Ni Co-Bridging with MoS2 Nanosheets for Enhanced Electrocatalytic Hydrogen Evolution Reactions. *RSC Adv.* **2018**, *8* (7), 3374−3380.
(34) Fakhri, A.; Nejad, P. A. Antimicrobial, Antioxidant and Cytotoxic Effect of Molybdenum Trioxide Nanoparticles and Application of This for Degradation of Ketamine under Different Light Illumination. *J. Photochem. Photobiol. B* **2016**, *159*, 211−217.
(35) Akhtar, M. J.; Ahamed, M.; Alhadlaq, H. A.; Alshamsan, A.; Majeed Khan, M. A.; Alrokayan, S. A. Antioxidative and Cytoprotective Response Elicited by Molybdenum Nanoparticles in Human Cells. *J. Colloid Interface Sci.* **2015**, *457*, 370−377.
(36) Zollfrank, C.; Gutbrod, K.; Wechsler, P.; Guggenbichler, J. P. Antimicrobial Activity of Transition Metal Acid MoO3 Prevents Microbial Growth on Material Surfaces. *Mater. Sci. Eng. C* **2012**, *32* (1), 47−54.
(37) Xing, Y.; Cai, Y.; Cheng, J.; Xu, X. Applications of Molybdenum Oxide Nanomaterials in the Synergistic Diagnosis and Treatment of Tumor. *Appl. Nanosci.* **2020**, *10* (7), 2069−2083.
(38) Desai, N.; Mali, S. Chemically Grown MoO3 Nanorods for Antibacterial Activity Study. *J. Nanomed. Nanotechnol.* **2015**, *06* (06), No. 1000338, DOI: 10.4172/2157-7439.1000338.
(39) De Foggi, C. C.; De Oliveira, R. C.; Assis, M.; Fabbro, M. T.; Mastelaro, V. R.; Vergani, C. E.; Gracia, L.; Andrés, J.; Longo, E.; Machado, A. L. Unveiling the Role of β-Ag2MoO4Microcrystals to the Improvement of Antibacterial Activity. *Mater. Sci. Eng. C* **2020**, *111*, No. 110765.
(40) Huang, F.; Gao, Y.; Zhang, Y.; Cheng, T.; Ou, H.; Yang, L.; Liu, J.; Shi, L.; Liu, J. Silver-Decorated Polymeric Micelles Combined with Curcumin for Enhanced Antibacterial Activity. *ACS Appl. Mater. Interfaces* **2017**, *9* (20), 16880−16889.
(41) Wang, J.; Li, T.; Yan, T.; Wei, X.; Qu, X.; Yuan, S. Friction Behavior of Silver Perrhenate in Oil as Lubricating Additive for Use at Elevated Temperatures. *Materials* **2019**, *12* (13), No. 2199, DOI: 10.3390/ma12132199.
(42) Imran, M.; Yousaf, A. B.; Farooq, M.; Kasak, P. Enhancement of Visible Light-Driven Hydrogen Production over Zinc Cadmium Sulfide Nanoparticles Anchored on BiVO4 Nanorods. *Int. J. Hydrogen Energy* **2022**, *47* (13), 8327−8337.
(43) Niu, Z.; Zhou, C.; Wang, J.; Xu, Y.; Gu, C.; Jiang, T.; Zeng, S.; Zhang, Y.; Ang, D. S.; Zhou, J. UV-Light-Assisted Preparation of MoO3−x/Ag NPs Film and Investigation on the SERS Performance. *J. Mater. Sci.* **2020**, *55* (21), 8868−8880.
(44) Dobias, J.; Bernier-Latmani, R. Silver Release from Silver Nanoparticles in Natural Waters. *Environ. Sci. Technol.* **2013**, *47* (9), 4140−4146.
(45) Shao, P.; Chang, Z.; Li, M.; Lu, X.; Jiang, W.; Zhang, K.; Luo, X.; Yang, L. Mixed-Valence Molybdenum Oxide as a Recyclable Sorbent for Silver Removal and Recovery from Wastewater. *Nat. Commun.* **2023**, *14* (1), No. 1365.
(46) Kim, T. I.; Kwon, B.; Yoon, J.; Park, I. J.; Bang, G. S.; Park, Y. K.; Seo, Y. S.; Choi, S. Y. Antibacterial Activities of Graphene Oxide-Molybdenum Disulfide Nanocomposite Films. *ACS Appl. Mater. Interfaces* **2017**, *9* (9), 7908−7917.
(47) Farooq, M.; Khalid, M.; Yoshinori, Y.; Wang, F.; Iqbal, M. A.; Sarwar, M. N.; Mayakrishnan, G.; Kim, I. S. Ag and MoO3 Nanoparticle-Containing Polyacrylonitrile Nanofiber Membranes for Wound Dressings. *ACS Appl. Nano Mater.* **2023**, *6*, 17171−17178, DOI: 10.1021/acsanm.3c03435.
(48) Wei, J.; Jiao, X.; Wang, T.; Chen, D. Electrospun Photochromic Hybrid Membranes for Flexible Rewritable Media. *ACS Appl. Mater. Interfaces* **2016**, *8* (43), 29713−29720.
(49) He, J.-H.; Wan, Y.-Q.; Yu, J.-Y. Effect of Concentration on Electrospun Polyacrylonitrile (PAN) Nanofibers. *Fibers Polym.* **2008**, *9* (2), 140−142.
(50) Oliveira, C. A.; Volanti, D. P.; Nogueira, A. E.; Zamperini, C. A.; Vergani, C. E.; Longo, E. Well-Designed β-Ag2MoO4 Crystals with Photocatalytic and Antibacterial Activity. *Mater. Des.* **2017**, *115*, 73−81.

https://doi.org/10.1021/acsomega.3c08814
ACS Omega 2023, 8, 49467−49477

(51) Fleisch, T. H.; Mains, G. J. An XPS Study of the UV Reduction and Photochromism of MoO3 and WO3. *J. Chem. Phys.* **1982**, *76* (2), 780−786.
(52) Chang, L.; Duan, L.; Sheng, M.; Yuan, J.; Yi, H.; Zou, Y.; Uddin, A. Optimising Non-Patterned MoO3/Ag/MoO3 Anode for High-Performance Semi-Transparent Organic Solar Cells towards Window Applications. *Nanomaterials* **2020**, *10*, 1759.
(53) Shafaei, S.; Dörrstein, J.; Guggenbichler, J. P.; Zollfrank, C. Cellulose Acetate-Based Composites with Antimicrobial Properties from Embedded Molybdenum Trioxide Particles. *Lett. Appl. Microbiol.* **2017**, *64* (1), 43−50.
(54) Walton, K. S.; Snurr, R. Q. Applicability of the BET Method for Determining Surface Areas of Microporous Metal-Organic Frameworks. *J. Am. Chem. Soc.* **2007**, *129* (27), 8552−8556.
(55) Lee, J.; Kim, J. G.; Chang, J. Y. Fabrication of a Conjugated Microporous Polymer Membrane and Its Application for Membrane Catalysis. *Sci. Rep.* **2017**, *7* (1), No. 13568.
(56) Ullah, A.; Saito, Y.; Ullah, S.; Haider, M. K.; Nawaz, H.; Duy-Nam, P.; Kharaghani, D.; Kim, I. S. Bioactive Sambong Oil-Loaded Electrospun Cellulose Acetate Nanofibers: Preparation, Characterization, and in-Vitro Biocompatibility. *Int. J. Biol. Macromol.* **2021**, *166*, 1009−1021.
(57) Alam, M. W.; BaQais, A.; Mir, T. A.; Nahvi, I.; Zaidi, N.; Yasin, A. Effect of Mo Doping in NiO Nanoparticles for Structural Modification and Its Efficiency for Antioxidant, Antibacterial Applications. *Sci. Rep.* **2023**, *13* (1), No. 1328.
(58) Özyürek, M.; Güngör, N.; Baki, S.; Güçlü, K.; Apak, R. Development of a Silver Nanoparticle-Based Method for the Antioxidant Capacity Measurement of Polyphenols. *Anal. Chem.* **2012**, *84* (18), 8052−8059.
(59) Sudha, A.; Jeyakanthan, J.; Srinivasan, P. Green Synthesis of Silver Nanoparticles Using Lippia Nodiflora Aerial Extract and Evaluation of Their Antioxidant, Antibacterial and Cytotoxic Effects. *Resour.-Effic. Technol.* **2017**, *3* (4), 506−515.
(60) Mahalingam, S.; Govindaraji, P. K.; Solomon, V. G.; Kesavan, H.; Neelan, Y. D.; Bakthavatchalam, S.; Kim, J.; Bakthavatchalam, P. Biogenic Synthesis and Characterization of Silver Nanoparticles: Evaluation of Their Larvicidal, Antibacterial, and Cytotoxic Activities. *ACS Omega* **2023**, *8* (13), 11923−11930.
(61) Sharma, A.; Saini, A. K.; Kumar, N.; Tejwan, N.; Singh, T. A.; Thakur, V. K.; Das, J. Methods of Preparation of Metal-Doped and Hybrid Tungsten Oxide Nanoparticles for Anticancer, Antibacterial, and Biosensing Applications. *Surf. Interfaces* **2022**, *28*, No. 101641.
(62) Mikhailova, E. O. Silver Nanoparticles: Mechanism of Action and Probable Bio-Application. *J. Funct. Biomater.* **2020**, *11* (4), No. 84, DOI: 10.3390/jfb11040084.
(63) Tanasic, D.; Rathner, A.; Kollender, J. P.; Rathner, P.; Müller, N.; Zelenka, K. C.; Hassel, A. W.; Mardare, C. C. Silver-, Calcium-, and Copper Molybdate Compounds: Preparation, Antibacterial Activity, and Mechanisms. *Biointerphases* **2017**, *12* (5), No. 05G607, DOI: 10.1116/1.4996434.
(64) Song, M.; Zhao, Q.; Wang, X.; Shi, C.; Hu, X.; Li, J. A Hydrophilic/Hydrophobic Janus Membrane Used as Wound Dressings with Enhanced Antibacterial Properties. *Fibers Polym.* **2022**, *23* (9), 2511−2516.
(65) Wang, L.; Hu, C.; Shao, L. The Antimicrobial Activity of Nanoparticles: Present Situation and Prospects for the Future. *Int. J. Nanomed.* **2017**, *12*, 1227−1249.
(66) Wang, X.; Herting, G.; Wallinder, I. O.; Blomberg, E. Adsorption of Lysozyme on Silver and Its Influence on Silver Release. *Langmuir* **2014**, *30* (46), 13877−13889.
(67) Wang, Z.; Zhu, J.; Chen, L.; Deng, K.; Huang, H. Multifunctional Gold-Silver-Carbon Quantum Dots Nano-Hybrid Composite: Advancing Antibacterial Wound Healing and Cell Proliferation. *ACS Appl. Mater. Interfaces* **2023**, *15* (34), 40241−40254.
(68) Jatoi, A. W.; Jo, Y. K.; Lee, H.; Oh, S. G.; Hwang, D. S.; Khatri, Z.; Cha, H. J.; Kim, I. S. Antibacterial Efficacy of Poly(Vinyl Alcohol) Composite Nanofibers Embedded with Silver-Anchored Silica Nanoparticles. *J. Biomed. Mater. Res., Part B* **2018**, *106* (3), 1121−1128.
(69) Phan, D. N.; Dorjjugder, N.; Saito, Y.; Taguchi, G.; Ullah, A.; Kharaghani, D.; Kim, I. S. The Synthesis of Silver-Nanoparticle-Anchored Electrospun Polyacrylonitrile Nanofibers and a Comparison with as-Spun Silver/Polyacrylonitrile Nanocomposite Membranes upon Antibacterial Activity. *Polym. Bull.* **2020**, *77* (8), 4197−4212.
(70) Lu, D. R.; Abu-Izza, K.; Mao, F. Nonlinear Data Fitting for Controlled Release Devices: An Integrated Computer Program. *Int. J. Pharm.* **1996**, *129* (1−2), 243−251.

https://doi.org/10.1021/acsomega.3c08814
ACS Omega 2023, 8, 49467−49477